

Modeling of the Residence Time Distribution in a Continuous Electrode Slurry Mixing Process in Battery Cell Production

Simon Otte,* Sebastian Schabel, and Jürgen Fleischer

Battery cell production is costly, especially due to expensive raw materials and high scrap rates, making continuous process optimization essential. Electrode manufacturing, particularly the mixing process that defines the fundamental electrochemical properties of a battery, offers great potential for increasing material efficiency. Understanding the residence time and residence time distribution (RTD) of particles within the continuous mixing process is crucial for optimization. Autonomous process control requires accurate prediction of the RTD to enable precise and resource-efficient rejection of nonconforming material. Similarly, knowledge of the RTD is required to ensure the traceability of battery cell materials within the mixing process. A model developed from experimental data is presented that simulates the RTD of a twin-screw extruder based on the input process parameters screw speed, mass flow, and solid content. This is possible for the entire system and the subsystems process section, solvent dosing unit, binder dosing unit, and powder dosing unit. As a result, the characteristic times can be predicted with a very high degree of accuracy from when the raw materials are added to the final slurry at the end of the continuous mixing process. This enables resource-efficient production and provides detailed information for traceability in continuous mixing processes.

1. Introduction


Increasing demand for batteries, especially lithium-ion batteries, and expensive raw materials require continuous process optimization.^[1] Therefore, the focus is on efficient battery cell production. The important foundations for subsequent cell performance and quality are initially defined within the mixing process.^[2] In this process, active materials (AMs), binders, and conductive agents such as carbon black (CB) are dispersed in a solvent.^[3] Mixing primarily aims to break up agglomerates

and achieve a homogeneous slurry with the specified viscosity.^[1,4] The quality of the slurry is influenced by various factors, including the mixing techniques, equipment, mixing intensity, duration, and sequencing.^[4] The resulting slurry's rheological properties, such as the dynamic viscosity, are affected by the screw elements and their configuration. Further essential process parameters are screw speed, throughput, filling degree, and residence time distribution (RTD).^[5] In particular, the knowledge of the RTD is important to reject scrap while maximizing resource efficiency and ensuring traceability. The cost of a battery cell is largely the result of material costs (up to 75% of total costs), mainly due to the AMs.^[6–9]

To achieve a high resource efficiency, low scrap rates, and high quality of the slurry, existing processes, such as the batch-based mixing process, can be optimized. Therefore, continuous slurry mixing offers great potential. In a continuous process, input materials are fed into the system continuously, undergoing chemical or physical transformations, and output materials are continually discharged.^[10] Twin-screw extruders (TSE) are particularly well suited for continuous mixing processes, offering several advantages over batch processes, like reduced processing time within minutes instead of hours. TSEs also provide optimized shear rates, greater product consistency, and reduced material waste. Additionally, TSEs allow higher output with lower space requirements.^[4,7,11,12] The knowledge of the RTD is relevant for autonomous process control, process optimization, or traceability of battery cells and their components. However, the RTD in the continuous mixing process of electrode slurry as a whole, but also in the individual subsystems, is unknown.

In the continuous mixing process, it is challenging to define product batches because there are no natural batches of material quantities. Therefore, complex materials and batch mixtures are created, and it is challenging to associate process data with the product.^[13–15] Batches and knowledge about the RTD are particularly relevant for two important scenarios: the material often can still be used for a certain period of time after an unexpected variation in the dosing unit since the consequences of the dosing oscillation do not reach the extruder outlet only after a certain dead time (t_{\min}) in production. It is not possible to eject

S. Otte, S. Schabel, J. Fleischer
wbk Institute of Production Science
Karlsruhe Institute of Technology
Kaiserstraße 12, 76131 Baden-Wuerttemberg, Germany
E-mail: simon.otte@kit.edu

 The ORCID identification number(s) for the author(s) of this article can be found under <https://doi.org/10.1002/ente.202500395>.

© 2025 The Author(s). Energy Technology published by Wiley-VCH GmbH. This is an open access article under the terms of the Creative Commons Attribution License, which permits use, distribution and reproduction in any medium, provided the original work is properly cited.

DOI: 10.1002/ente.202500395

nonconforming material precisely in a resource-efficient manner without knowing the residence time in the process. However, the traceability of slurry ingredients during the mixing process remains unresolved, as the traceability of battery cells and their components is currently only possible from the coating process onward. In addition, understanding the residence time of materials within the mixing process is critical for further process automation, autonomous process control, and to optimize both the process and the final product.

Therefore, knowledge of the residence time and RTD offers an advantage in several ways. Systematic investigations of the RTD in the continuous mixing process have already been carried out. The effect of relevant parameters like screw speed, mass flow, and solid content on the mean residence time t_m and the RTD have been studied.^[16] Based on these findings, a model was developed that allows the simulation of the RTD and the characteristic times t_{\min} , t_m , t_{peak} , and t_{\max} for the individual subsystems and the continuous process for the first time. A final model validation shows a very high model and prediction quality.

2. Background

The RTD is a fundamental parameter for understanding mixing behavior and the efficiency of continuous processes in chemical engineering and process analysis. It describes the RTD that fluid elements spend in a reactor or a continuous mixing system and provides a probability distribution of the residence times of fluid particles within the system.^[17] The distribution function $E(t)$ mathematically represents the temporal distribution of material elements within the system. To obtain a probability distribution, $E(t)$ is normalized to ensure its total area equals one.^[18]

An RTD model can be developed by experimentally determining the RTD using a tracer and modeling the RTD curves mathematically. Various model equations are used to represent the behavior of the RTD. In fluid dynamics, models are broadly categorized as ideal or real. The primary ideal models are the plug flow reactor (PFR) and the continuous stirred-tank reactor (CSTR). The PFR represents a system where the input concentration is delayed without mixing. The tracer concentration curves at the inlet and outlet are identical, differing only by a time shift Δt .^[19] Physically, this implies that elements entering the reactor simultaneously travel along parallel paths at a constant velocity, leaving at the same time.^[17] In contrast, a CSTR assumes complete mixing of the fluid or powder. The RTD for a CSTR is described by the equation

$$E(t) = \frac{1}{t_m} * e^{-t/t_m} \quad (1)$$

where t_m is the mean residence time. This function indicates that the highest probability for residence time occurs at $t = 0$ s.

Real systems show flow behavior that lies between PFR and CSTR due to phenomena such as dead zones, channeling effects, and circulations.^[20] As a result, it is necessary to combine idealized models or use alternative models to describe the behavior of real systems accurately. In an ideal laminar pipe flow, molecular diffusion is neglected and fluid elements follow different trajectories dictated by the Hagen–Poiseuille velocity profile.^[19] The RTD for such a flow is described by

$$f(t) = \frac{t_m^2}{2 * t^3} f \text{ or } t > t_m \quad (2)$$

and $f(t) = 0$ otherwise, where $t_m = \frac{\dot{m}}{V}$ with \dot{m} as the mass flow rate and V as the system volume. The cascade of stirred tanks model represents a series of N ideal CSTRs. The RTD for the entire system is given by

$$E(\theta) = \frac{N * (N * \theta)^{N-1}}{(N-1)!} * e^{-N*\theta} \quad (3)$$

where θ is the dimensionless time. By adjusting N , the experimentally determined RTD can be approximated. For $N \rightarrow \infty$, the RTD approaches that of a PFR, while $N = 1$ represents a single CSTR.^[21] Additional model equations can be obtained by combining CSTRs and PFRs in various configurations. The axial dispersion model accounts for molecular diffusion and turbulent flow effects, such as velocity fluctuations and vortex formation.^[22] The dimensionless RTD equation for this model, with open boundary conditions, is

$$E(\theta) = \sqrt{\frac{Pe}{4\pi * \theta}} \exp\left(-\frac{Pe * (1 - \theta)^2}{4\theta}\right) \quad (4)$$

where θ is the dimensionless time and Pe is the Péclet number. The Péclet number indicates the ratio of convective to dispersive transport, reflecting the degree of dispersion in the system. A high Pe value corresponds to low dispersion and poor axial mixing, while a low Pe value indicates high dispersion and efficient axial mixing. When $Pe = 0$, the system behaves as a perfectly mixed CSTR, and as $Pe \rightarrow \infty$ it approaches PFR behavior.^[23]

3. State of the Art

RTD is a fundamental parameter in the design and optimization of industrial processes, particularly in the food and pharmaceutical sectors. Understanding RTD allows for predicting how long materials spend time in a system, which is essential for ensuring product quality and process efficiency. Over the years, various mathematical models have been developed to analyze RTD, leading to significant advancements in the field.

Nassauer laid the groundwork for RTD modeling by using various mathematical approaches to study fluid flow in systems such as pipelines and reactors. He established an empirical relationship between RTD and mean residence time by modifying the turbulent flow model by neglecting diffusion effects. This fundamental work was later extended by integrating a dispersion model that included an effective mean velocity, providing a more accurate representation of fluid dynamics in turbulent environments.^[24]

Salamí (1968) combined a dispersion model with a stirred tank cascade model, which improved the fitting of RTD and enabled the representation of asymmetric distributions.^[25] However, as noted by Ham and Platzer (2004), fitting real curves with a single parameter can be challenging. They proposed two semiempirical RTD models based on two or three parameters, emphasizing that at least two parameters are necessary for a good fit.^[26]

Hart and Guymer et al. (2016) further advanced the field by investigating the RTD of laminar and turbulent pipe flows through variations in the Reynolds number using fluorescence measurements. Their mathematical modeling demonstrated that Danckwerts' equation (1953) provides a reliable approximation of the experimentally determined RTD for ideal laminar flow.^[27]

In the context of powders and granulates, mathematical modeling is essential for optimizing processes in the food and pharmaceutical industries. Peterwitz and Jodwirschat (2022) established empirical models to analyze RTD in a tablet production system, focusing on the effects of back-mixing in the feeder.^[28] Bhalode and Razavi (2023) utilized axial dispersion models to fit RTD curves from experiments with varying tracer concentrations, highlighting the significance of careful tracer selection and addition methods for accurate modeling. Their work in 2024 further refined these models, reinforcing the importance of these factors in RTD analysis.^[29]

Gao and Walsh (1999) developed a predictive RTD model for polymer extrusion and investigated the influence of the parameters mass flow and rotational screw speed. They showed that the mass flow significantly influences the residence time and showed that the RTD does not change with specific throughput. This highlights the necessity for dynamic modeling in process optimization.^[30] Similarly, Razavi and Román-Ospino (2023) conducted a systematic comparison of different tracer materials, employing multivariate analysis of variance to validate their findings, thereby reinforcing the importance of statistical methods in RTD modeling.^[31]

Escotet-Espinoza and Moghtadernejad (2019) differentiated between model-based and nonmodel-based approaches for RTD analysis, emphasizing the need for careful experimental design and data processing to ensure accurate results.^[32,33]

Van Snick and Kumar (2019) developed an RTD model for a feeder based on material and process parameters, using near-infrared technology to determine maximum residence times. They stressed the significance of material properties in influencing RTD, indicating that different feeders may require tailored modeling approaches.^[34]

Engisch and Muzzio (2016) further contributed to the understanding of RTD by analyzing the individual components of a production system and calculating the overall RTD using established equations. Their findings revealed significant differences in RTD distributions among components, which is crucial for effective process design.^[35]

The literature research shows that no prediction model has been created for the RTD in the continuous mixing process of the battery slurry. Compared to the pharmaceutical and food industries, the experimental RTD determination is also not adequately investigated. In addition, it has not been determined which powder properties are important for the development of an RTD model. Therefore, developing an empirical model using experimental data is unavoidable, as the RTD is influenced by material properties, system components, and process parameters.

4. Materials and Experimental Setup

A TSE ZSK 18 MEGAlab (ZSK 18Ml) (Coperion GmbH, Germany) was used to study the RTD in the continuous mixing

process. This TSE can be divided into several subsystems, as shown in **Figure 1**. There are two liquid dosing units for the solvent water (blue) and a mixture of solvent and styrene-butadiene rubber (SBR) binder (blue) with identical design. They consist of a tank and an extruder screw pump (type NM005BY) from Netzsch (Germany). After the pump, there is a hose connection to the process section. The powder dosing unit (khaki) consists of a hopper with an agitator for homogenization. For gravimetric powder dosing, twin-screws are used (type Pharma QT20 version, Coperion GmbH, Germany).

The core of the system is the ZSK 18Ml TSE. The two screws rotate in the same direction and consist of kneading, shearing, back-mixing, and conveying elements with different pitches. The screw configuration was not changed during the experiments. The conductivity of the slurry at position Z (Figure 1) was measured with a conductivity sensor type 8221 (Christian Bürkert GmbH & Co. KG, Germany).

The processed water-based anode slurry uses Mechano-Cap1P1 graphite (HC Carbon GmbH, Germany) as AM. Its conductivity is improved by adding Super C65 conductive CB (Nanografi Nano Technology, Turkey). Binders and additives are also used to maintain the stability of the electrode microstructure during production and cell operation. In this case, a carboxymethyl cellulose (Carl Roth, Germany) and a SBR solution with a degree of substitution of 0.85 (Nanografi Nano Technology, Turkey) were used as binders.

The RTD experiments based on a Box Behnken Design (BBD) of experiment (see appendix **Table 7**) were performed under controlled conditions to minimize external disturbances. The process section temperature of the TSE was kept constant at 22.5 °C. To minimize variations in feed homogeneity, all experiments were performed with a single batch of dry components. Before each experiment, the hoppers were completely filled to ensure that the entire experiment could be completed without refilling. Also, the TSE processed untraced powders for at least two average residence times to ensure stable operating conditions. The process and machine parameters as well as the conductivity sensor data were collected using a Siemens Simatic S7-1500 PLC and accessed through an OPC UA interface. A self-developed data logging tool, implemented with MATLAB R2021a (The MathWorks Inc., USA), was used to record the data at a rate of 10 Hz. Further details on tracer selection and the detailed procedure for determining the curves and interpreting the RTD are presented in Otte et al. 2025.^[16]

5. Own Approach and Methodology

The RTD model uses three process parameters as factors: the screw speed n , the solid content f of the slurry, and the mass flow rate \dot{m} of the slurry. Each material (deionized water, binder solution, and premix) has a different RTD in the TSE due to their different material flow paths and properties. This is why the RTD model is divided into four subsystems, as illustrated in Figure 1 and **Table 1**: solvent dosing unit (blue), binder dosing unit (green), powder dosing unit (khaki), and process section (red).

A 1 mol L⁻¹ NaCl solution was used as a tracer for the experiments. A conductivity sensor was used to measure the

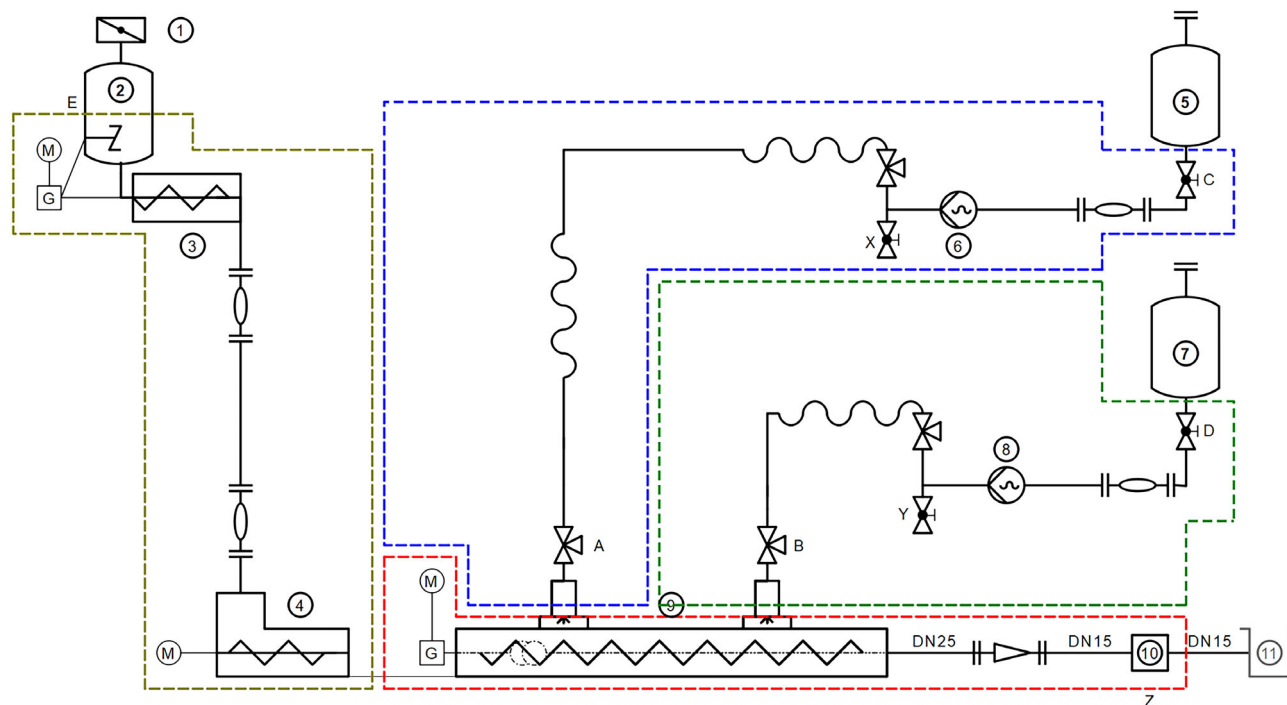


Figure 1. P&I diagram of the TSE with the subsystem solvent dosing unit (blue), binder dosing unit (green), powder dosing unit (khaki), and process section/TSE (red). 1 = double valve system; 2 = premix hopper; 3 = dosing screw; 4 = side feeder (ZSB); 5 = solvent tank; 6 = eccentric screw pump solvent; 7 = binder solution tank; 8 = eccentric screw pump binder solution; 9 = process section with twin screw; 10 = conductivity sensor; 11 = slurry container; A = solvent addition point; B = binder solution addition point; C = tracer addition point solvent dosing unit; D = tracer addition point binder dosing unit; X = conductivity measuring point for solvent; Y = conductivity measuring point for binder solution; Z = conductivity measuring point for process section and powder dosing unit.

Table 1. Overview of process parameters and modeling approaches for the four subsystems.

Material	Subsystem	Process parameter	Modeling approach
Solvent (water)	Process section	\dot{m}_{slurry}, n, f	Experimentally
	Solvent dosing unit	\dot{m}_{water}	Experimentally
	Hose	\dot{m}_{water}	Experimentally
Binder solution	Process section	\dot{m}_{slurry}, n, f	Experimentally
	Binder dosing unit	\dot{m}_{SBR}	Experimentally
	Hose	\dot{m}_{SBR}	Experimentally and analytic
Premix	Powder dosing unit	\dot{m}_{Premix}	Experimentally
Extruder	Process section	\dot{m}_{slurry}, n, f	Experimentally

conductivity variations over time at defined experimental points to determine the tracer concentration at the extruder outlet and thus the RTD. For each experimental point, the mass flow rate, screw speed, and solid content were varied. Three RTD curves for slurry within the TSE were recorded to minimize the impact of individual measurement errors. Tracer addition is repeated after the baseline conductivity of the slurry is stable for at least a time

period of twice t_m .^[16] The measured conductivity curve is normalized between 0 and 1 to remove the background conductivity and to isolate the effect of the tracer. Normalization also compensates for differences in medium properties, such as solid content, that affect absolute conductivity. Finally, the conductivity curve is area normalized to 1, converting it to a probability distribution for RTD analysis and modeling.

The next step is to mathematically model the normalized conductivity curves. The exponentially modified Gaussian (EMG) from the Origin 2024b software by OriginLab Corporation is used:

$$f(t) = \gamma_{01} + (f_1 * f_2)(t) \quad (5)$$

$$f_1(t) = \frac{A}{t_0} e^{-\frac{t}{t_0}} \quad (6)$$

$$f_2(t) = \frac{1}{\sqrt{2 * \pi w}} e^{-\frac{(t-x_c)^2}{2w^2}} \quad (7)$$

The EMG has the parameters γ_0 for the shift of the y -axis, A for the area under the curve, x_c for the center, w for the width and the constant t_0 . Both the width w and $t_0 > 0$ must be lower limits. There is no upper limit. **Figure 2** shows an example of the fitting of the EMG to the normalized and averaged conductivity curve of the center point of the process section. The meaning of the EMG parameters is also shown graphically. The Levenberg–Marquardt

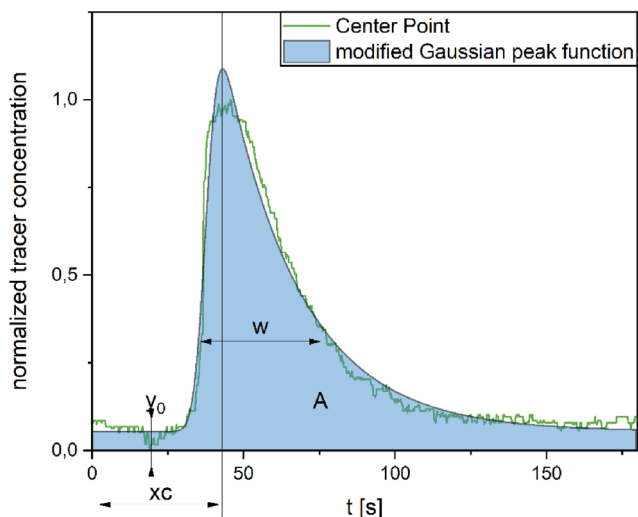


Figure 2. Comparison of the measured conductivity curve (green) and the modeled conductivity curve (blue) for the center point.

algorithm determines the parameters A , x_c , w , t_0 , and y_0 of the displayed conductivity curve.

The curve parameter y_0 is calculated but set to zero for further modeling as a shift in the y -axis is not relevant for distribution curves. This is because distribution curves converge to zero as $t \rightarrow \infty$ and $t = 0$ s and therefore do not show a constant shift.

The obtained parameters, together with Equation (5)–(7), form the basis of the RTD model of the respective subsystem. These parameters only depend on the corresponding input parameters.

5.1. RTD Model Setup for Process Section

The RTD models for the process section represent the RTD for the time any element spends from entering the TSE through the twin screws to the outlet at position Z (Figure 1). The parameters of the selected EMG function (Equation (5)–(7)) are determined using the software’s Levenberg–Marquardt algorithm, which combines the Gauss–Newton method with the gradient descent method. A quadratic correlation is assumed. For each curve parameter of the EMG, the following equation is developed:

$$y = a_0 + a_1 \dot{m} + a_2 n + a_3 f + a_4 \dot{m}^2 + a_5 n^2 + a_6 f^2 + a_7 \dot{m}n + a_8 \dot{m}f + a_9 nf \quad (8)$$

Initially, the statistical significance of all terms is evaluated. If a term shows no statistically significant association with the dependent variable, it is removed stepwise to simplify the regression model. This reduction process improves model simplicity and simulation accuracy.

The RTD of fluids in the liquid dosing unit is mathematically modeled using the software Origin 2024b from OriginLab Corporation. For the liquid dosing unit, an exponential function is selected. To build the simulation model, the mathematical relationship between the parameters of the curve and the mass flows of the fluids is determined and validated. The center of the factor space is chosen as the validation point.

5.2. RTD Model Setup for Solvent Dosing Unit and Binder Dosing Unit

The technical unit for dosing the solvent and the binder solution are identical in construction and have no technical differences. The only difference between the two systems is the medium being dispensed. Due to the technically identical design, the same procedure can be used to develop the RTD model for this subsystem. Therefore, the subsystems will only be distinguished in the formulas below, but not in the explanation of the procedure. If no distinction is necessary or if a statement concerns both the solvent dosing unit and the binder dosing unit, the term liquid dosing unit is used.

The RTD models for the liquid dosing units represent the time an element travels through the entire system, from the tank to the inlet of the TSE. The water-solvent RTD model characterizes the mass flow starting at the bottom of the water tank (5) and ending at the inlet at location A. The binder solution simulation model system boundary starts at the bottom of the binder solution tank (7) and ends at the inlet at location B. The RTD model is developed by experimentally determining the RTD for the fluid in the liquid dosing unit, the connecting hose to the TSE, and is based on the EMG (Formula (5)–(7)). The total RTD is then calculated by convolving the RTDs of each subsystem in order of flow direction. The RTDs are determined experimentally separately due to different flow characteristics and entry points into the TSE (Figure 1).

5.3. RTD Model Setup for Premix

The modeling of the powder dosing unit followed basically the same approach as the modeling of the other subsystems. However, the RTD analysis for this subsystem showed a bimodal curve with two peaks. The first peak has a significant amplitude and a small spread, while the second peak follows at a greater distance, has a significantly smaller amplitude, and is more widely spread.^[16] There is a core flow in the feeder and the powder dosing unit. A three-bladed agitator rotating around a horizontal axis is used to prevent powder bridges and reduce segregation. The first peak is caused by material that follows the core flow and passes the agitator without significant interaction. The second peak is caused by material that interacts with the agitator, i.e., it is transported upward into the hopper against the core flow direction. Due to the bimodal curve, the following basic term applies:

$$E(t) = t_0 + f_{1,Peak1}(t) + f_{1,Peak2}(t) \quad (9)$$

As with the other submodels, each peak term is described by the four parameters A , x_c , w , and t_0 . The insertion of Equation (6) and (7) results in the following equation with the constant g , which does not depend on \dot{m}_{premix} :

$$E(t) = t_0 + \frac{A_1}{\sqrt{2\pi} * w_1} * e\left(\frac{-(t-x_{c1})^2}{2 * \left(\frac{w_1}{g}\right)^2}\right) + \frac{A_2}{\sqrt{2\pi} * w_2} * e\left(\frac{-(t-x_{c2})^2}{2 * \left(\frac{w_2}{g}\right)^2}\right) \quad (10)$$

6. Modeling of Residence Time Distribution

This section presents the models for the individual subsystems. Each subsection describes the respective model and its specialties.

6.1. RTD Model of the Process Section

The submodel of the process section is the core of the entire RTD model. In addition to mixing due to the flow behavior of the medium, there is also an active mixing process, which is defined by the chosen screw configuration. Mass flow, screw speed, and solid content are the variable parameters used as input to the process section RTD model. The response curves of the system were analyzed for all experimental points and a curve fit was carried out according to the procedure described in Section 5.

An analysis using contour plots shows how the three key process parameters screw speed, mass flow, and solid content affect the RTD in the TSE (Figure 3). At low solid content, the residence time is shorter and almost independent of screw speed. At low screw speed and high solid content, the residence time increases. Overall, the shortest residence time occurs at high screw speed and high mass flow, while the longest occurs at low values of these parameters. Additionally, mass flow and solid content have a larger influence on the shift of the RTD curve than screw speed. The width of the RTD curve increases with high solid content.

Screw speed has a smaller effect than mass flow. High screw speed combined with high mass flow results in a narrow RTD curve, indicating little back mixing in the process.

Based on the results of the analysis, the model is set up. The coefficients of the regression model indicate the influence of the process parameters on the curve parameters of the EMG. The curve parameters are the response variables of the regression model with the process parameters as effects. The coefficients are determined using Minitab 22.1 software from Minitab GmbH (Germany). The regression model consists of the main effects of mass flow, solid content, and screw speed as well as their quadratic terms and the two-factor interactions. No weighting is chosen to calculate the coefficients and a two-sided 95% confidence interval is set.

Figure 4 shows the results of the stepwise regression of the model for the BBD with the absolute values of the effects in Pareto plots. Pareto plots are used to determine the effects of the regression model that contribute the most to the spread of the response variable. The larger the blue bar, the greater the influence on the response variable. In stepwise regression, effects are identified for which the statistical significance is less than the 0.05 significance level. The threshold is calculated using the significance level α . The reference line for statistical significance in the Pareto plot is drawn at the $(1 - \alpha/2)$ th quantile of a t -distribution with degrees of freedom for the error term^[36]. All effects below the threshold (red reference line), and shown with

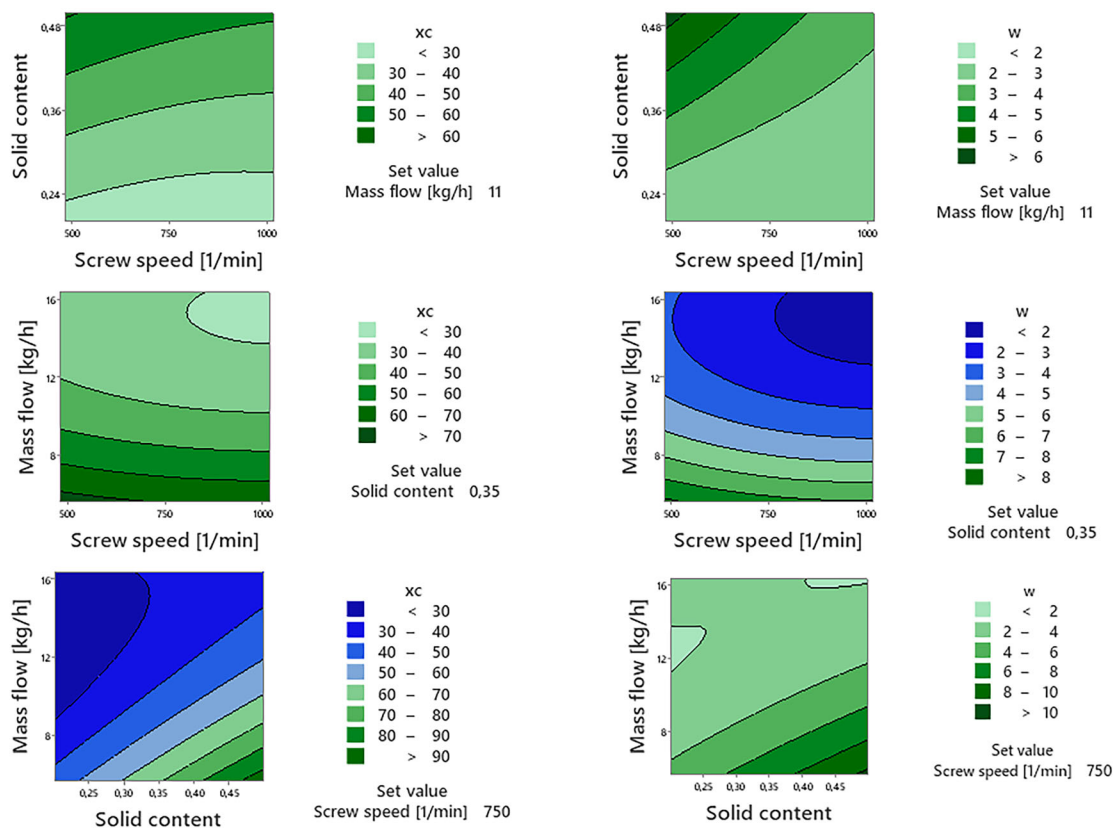


Figure 3. Contour plots of the parameters w and xc visualizing the dependencies of the process parameters of the TSE based on the BBD experimental design.

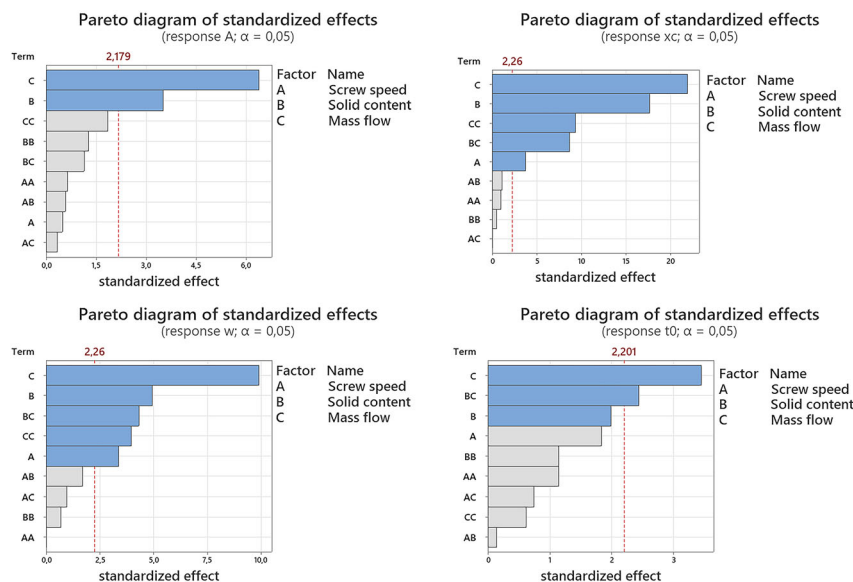


Figure 4. Pareto diagram of the standardized effects of the regression model of the process section for the BBD.

a gray bar, are not statistically significant. For the response variable *A*, only the effects of solid content and mass flow are statistically notable. Screw speed and the two-factor interactions do not have a statistically relevant effect on response variable *A* because their standardized effect is less than the threshold of 2.179. The response variable *xc* also depends on the quadratic effect of mass flow, the interaction of solid content and mass flow, and the screw speed. The same applies to response *w*. Again, mass flow has the strongest effect on the response. For the response variable *t₀*, the solid content, the mass flow, and the interaction of these two variables are statistically significant. Overall, mass flow has the greatest influence on the four response variables.

The coefficient values for the statistically significant effects for determining the RTD in the TSE are shown in **Table 2**. The larger a coefficient, the greater the influence of that effect on the response variable. For a negative coefficient, the influence quantity decreases the curve parameter. Empty cells in the table symbolize effects that are not significant.

Table 2. Coefficients of the regression model for the BBD and its significant effects.

Coefficients	<i>A</i>	<i>xc</i>	<i>w</i>	<i>t₀</i>
Constant	35.36	50.24	6.82	40.41
Screw speed	–	–	–0.01	0.00
Solid content	35.50	251.30	32.65	–40.40
Mass flow	–1.89	–8.00	–1.00	–2.55
Screw speed ²	–	–	–	–
Solid content ²	–	–	–	–
Mass flow ²	–	0.42	0.06	–
Screw speed * Solid content	–	–	–	–
Screw speed * Mass flow	–	–	–	–
Solid content * Mass flow	–	–13.43	–2.13	5.10

To analyze the quality of the regression models, the coefficient of determination R^2 and the standard deviation σ are calculated. These statistical measures are summarized in **Table 3**. As shown, the simulation model based on the BBD is very accurate. Only for the response variable *t₀* is the expected accuracy slightly lower.

Residual plots for each response variable are used to examine the fit of the selected regression model. **Figure 5** shows a probability plot for the residuals of the response variable *t₀* for the BBD regression model on the left. On the right is a plot of the residuals versus the adjustments. These plots are used to assess whether the residuals from a model are normally distributed (left plot) and whether there are patterns in the residuals that may indicate model fitting problems (right plot). The blue dots in the plots represent the residuals from the experiment points.

In the left plot, points near the dashed line indicate that the residuals are approximately normally distributed.

In the right plot in **Figure 5**, the residuals are plotted against the fitted values. The adjusted values are greater than 15 for all experiment points, except experiment point BBD7. Since the residual of BBD7 is close to zero, it is not an outlier, but rather an influential experiment point. A measurement error could be excluded. The spread of the other experiment points is large and no pattern can be seen. This indicates a good model fit with no constant variance. Therefore, the BBD regression model is

Table 3. Accuracy of fit of the model parameters of the BBD experimental design.

Parameter	<i>A</i>	<i>xc</i>	<i>w</i>	<i>t₀</i>
σ	4.48	2.47	0.78	3.33
R^2	81.64%	99.08%	94.92%	66.39%
R^2_{cor}	78.57%	98.57%	92.10%	57.22%
R^2_{prog}	72.43%	96.52%	84.63%	45.07%

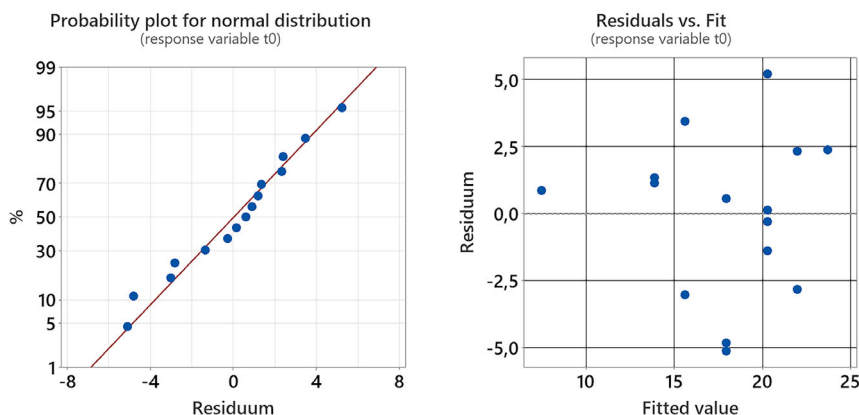


Figure 5. Residual diagram for a curve parameter for a single experimental point from the BBD.

suitable for building the prediction model to determine the RTD in the mixing process in the TSE.

The following formula is developed for the RTD model of the subsystem process section based on the presented results and uses formula (5)–(7) as a basis:

$$E(t)_{process\ section} = \frac{A}{t_0} * \exp\left(0.5 * \left(\frac{w}{t_0}\right)^2 - \frac{t - xc}{t_0}\right) * \Phi\left(\frac{t - xc}{w} - \frac{w}{t_0}\right) \quad (11)$$

with

$$A = 35.36 + 37.5 * f - 1.894 * \dot{m} \quad (12)$$

$$xc = 50.24 - 0.0122 * n + 251.3 * f - 8 * \dot{m} + 0.4152 * \dot{m}^2 - 13.43 * f * \dot{m} \quad (13)$$

$$w = 6.82 - 0.00349 * n + 32.65 * f - 0.998 * \dot{m} + 0.0559 * \dot{m}^2 - 2.129 * f * \dot{m} \quad (14)$$

$$t_0 = 40.41 - 40.4 * f - 2.545 * \dot{m} + 5.1 * f * \dot{m} \quad (15)$$

and \dot{m} as mass flow, n as screw speed and f as solid content.

6.2. RTD Model of the Liquid System

Based on the BBD of experiment, the corresponding minimum, medium, and maximum mass flows for the liquid systems, in this case the solvent water and the binder-water solution, were defined (see **Table 4**).

Table 4. Mass flow rates for the liquid dosing unit of the solvent water (\dot{m}_{H_2O}) and binder solution (\dot{m}_{SBR}).

	\dot{m}_{H_2O}	\dot{m}_{SBR}
Min	1.15 kg h ⁻¹	0.17 kg h ⁻¹
Medium	5.41 kg h ⁻¹	1.10 kg h ⁻¹
Max	9.67 kg h ⁻¹	2.03 kg h ⁻¹

The evaluation of the residence time curves shows a very large difference between the RTD of \dot{m}_{min} and \dot{m}_{max} . With particularly long experimental times and the associated very slow and incremental drop of the curves, the resolution capability of the conductivity sensor leads to a step effect, which is why the procedure described in Section 5 was extended by an initial step of data preparation. Therefore, the conductivity curve is smoothed with a Gaussian filter with a mask size of 15. This low-pass filter suppresses the high-frequency measurement noise by folding it with a Gaussian bell curve^[37]. This filter is better suited than a moving average because the moving average shifts the curve to the right, affecting the residence time. The background conductivity, which is defined as the minimum conductivity measured during the recording of the curve to avoid negative conductivity values, is then subtracted (see **Figure 6**).

In order to set up the prediction model for determining the RTD in the liquid dosing units, a mathematical relationship between the four curve parameters A , xc , w , and t_0 from the EMG and the liquid mass flow is determined. By comparing

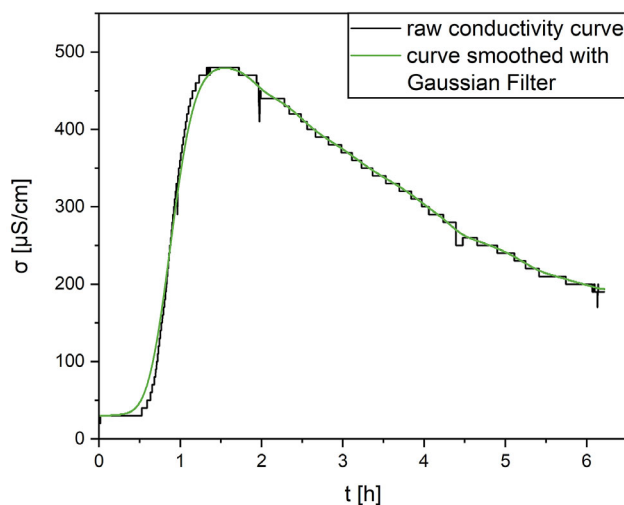


Figure 6. Comparison of the raw data of the conductivity curve with the smoothed conductivity curve of the binder solution in the liquid dosing unit.

the coefficient of determination R^2 of different regression equations, it became apparent that an exponential regression model is best suited. The exponential regression equation can be expressed with

$$y(t) = A_1 * \exp\left(-\frac{t}{t_1}\right) + \gamma_{02} \quad (16)$$

with offset γ_{02} , amplitude A_1 , and time constant t_1 . Again, the parameters γ_{02} , A_1 , and t_1 are determined using the Levenberg–Marquardt algorithm (Figure 7). An R^2 greater than 99.9% is obtained for all four parameters.

As the mass flow of the fluids (both demineralized water and binder solution) increases, the area of the curve characterized by the parameter A decreases. As the mass flow increases, κc decreases, which means that curve is shifted to the left toward shorter residence times. The width w of the curve also decreases with increasing mass flow. In summary, the higher the mass flow of the fluid, the shorter the residence time and the lower the back mixing. The RTD function, based on the EMG function, can be described for the liquid dosing of the solvent water as

$$E(t)_{Dosing, H_2O} = \frac{A_{H_2O}}{\sqrt{2\pi} * w_{H_2O}} * \exp\left(-\frac{(t - \kappa c_{H_2O})^2}{2 * \left(\frac{w_{H_2O}}{2.3548}\right)^2}\right) \quad (17)$$

with

$$A_{H_2O} = 84280.74561 + 1130492.1997 * \exp\left(-\frac{\dot{m}_{H_2O}}{2.04866}\right) \quad (18)$$

$$\kappa c_{H_2O} = 109.96393 + 981.81973 * \exp\left(-\frac{\dot{m}_{H_2O}}{2.54993}\right) \quad (19)$$

$$w_{H_2O} = 17.95708 + 128.90143 * \exp\left(-\frac{\dot{m}_{H_2O}}{3.79474}\right) \quad (20)$$

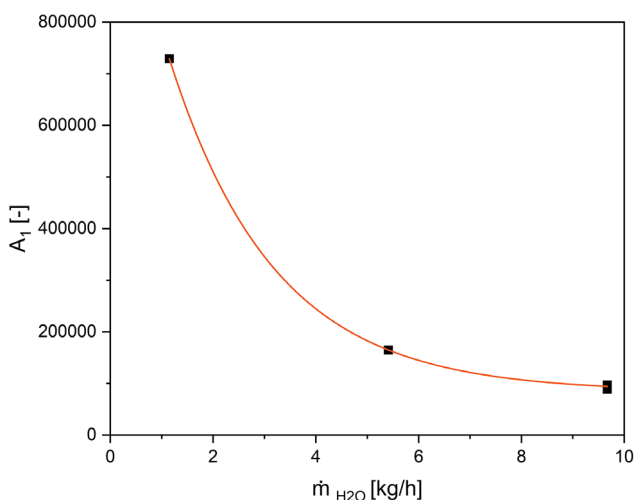


Figure 7. Representation of the mathematical relationship between \dot{m} and the parameter A . The black dots represent the parameter values determined by the experiment points, the orange curve formula (18).

The formula for the liquid dosing of the binder solution was developed using the same procedure as for the dosing of the solvent. $E(t)_{Dosing, SBR}$ can be described as follows:

$$E(t)_{Dosing, SBR} = \frac{A_{SBR}}{\sqrt{2\pi} * w_{SBR}} * \exp\left(-\frac{(t - \kappa c_{SBR})^2}{2 * \left(\frac{w_{SBR}}{2.3548}\right)^2}\right) \quad (21)$$

with

$$A_{SBR} = 198684.0382 + 1.24 * 10^7 * \exp\left(-\frac{\dot{m}_{SBR}}{0.42345}\right) \quad (22)$$

$$w_{SBR} = 56.09565 + 1480.62594 * \exp\left(-\frac{\dot{m}_{SBR}}{0.35031}\right) \quad (23)$$

$$\kappa c_{SBR} = 368.68343 + 4477.75181 * \exp\left(-\frac{\dot{m}_{SBR}}{0.42345}\right) \quad (24)$$

Based on findings in the literature, a formula for laminar flow in the connecting hose was first assumed. For a solvent hose diameter of 5 mm, a solvent hose length of 2.3 m, and a solvent density of 1000 kg m^{-3} , the following formula results for this flow behavior:

$$E(t)_{hose, old} = \frac{\left(\frac{3.7 * \left(\frac{5}{2}\right)^2 * \pi * \rho * 3.6}{\dot{m}_{H_2O} * 1000}\right)^2}{2t^3} \quad (25)$$

However, further investigations showed that this formula does not adequately describe the real conditions since additional mixing effects occurred. To take this effect into account, an empirically based on formula (7) is developed using the results of the experimental investigations and the mass flows shown in Table 4. This is as follows:

$$E(t)_{hose} = \frac{A_h}{\sqrt{2\pi} * w_h} * \exp\left(-\frac{(t - \kappa c_h)^2}{2 * \left(\frac{w_h}{2.3548}\right)^2}\right) \quad (26)$$

with

$$A_h = 17.7071 + 1747.77382 * \exp\left(-\frac{\dot{m}_{H_2O}}{1.19834}\right) \quad (27)$$

$$\kappa c_h = 23.07876 + 359.61072 * \exp\left(-\frac{\dot{m}_{H_2O}}{1.92491}\right) \quad (28)$$

$$w_h = 2.49772 + 123.37827 * \exp\left(-\frac{\dot{m}_{H_2O}}{1.20163}\right) \quad (29)$$

6.3. RTD Model of the Powder Dosing Unit

The bimodal curve of the powder dosing unit requires a modified model as shown in Section 5.3. Accordingly, eight curve parameters are considered, with four parameters (A , κc , w , and t_0) defined for each peak. These parameters were determined using the method described in Section 5. For the powder dosing unit, the following formula results:

$$E(t)_{\text{powder dosing unit}} = t_0 + \frac{A_1}{\sqrt{2\pi} * w_1} * \exp\left(-\frac{(t - xc_1)^2}{2 * \left(\frac{w_1}{2.3548}\right)^2}\right) + \frac{A_2}{\sqrt{2\pi} * w_2} * \exp\left(-\frac{(t - xc_2)^2}{2 * \left(\frac{w_2}{2.3548}\right)^2}\right) \quad (30)$$

with

$$A_1 = 2668.031 * e^{-0.531\dot{m}_{\text{premix}}} \quad (31)$$

$$w_1 = 2810.222 * e^{-0.533\dot{m}_{\text{premix}}} \quad (32)$$

$$xc_1 = 3334.296 * e^{-0.476\dot{m}_{\text{premix}}} \quad (33)$$

and

$$A_2 = 2612.231 * e^{-0.397\dot{m}_{\text{premix}}} \quad (34)$$

$$w_2 = 1993.850 * e^{-0.158\dot{m}_{\text{premix}}} \quad (35)$$

$$xc_2 = 27009.133 * e^{-0.631\dot{m}_{\text{premix}}} \quad (36)$$

The mass flow \dot{m}_{premix} is calculated according to the recipe and the set parameters.

6.4. RTD Model of the entire continuous mixing process

The model for calculating $E(t)$ for the entire TSE in the continuous mixing process is based on a combination of the presented submodels, as shown in **Figure 8**. These submodels are combined by convolution. For the calculation of $E(t)$, only the submodels along the relevant material flow path are considered. In addition, the characteristic times t_{min} , t_{peak} , t_m , and t_{max} are determined for both the individual subsystems and the overall system to allow a detailed analysis of the RTD.

7. Validation and Discussion

Validation is conducted separately for each subsystem. Afterward, the overall model is validated using the liquid dosing unit with water as the solvent, consisting of the subsystems solvent dosing unit, hose, and TSE. This scenario was chosen because most of the submodels have to be folded together, which makes the probability of deviations particularly high.

7.1. RTD Model Validation of the Process Section

To validate the RTD prediction model of the process section, new experiments were carried out after the model was created. To do this, experiment points within the RTD model space are selected and tracer measurements are taken. The prediction of the RTD in the mixing process in the TSE is validated using

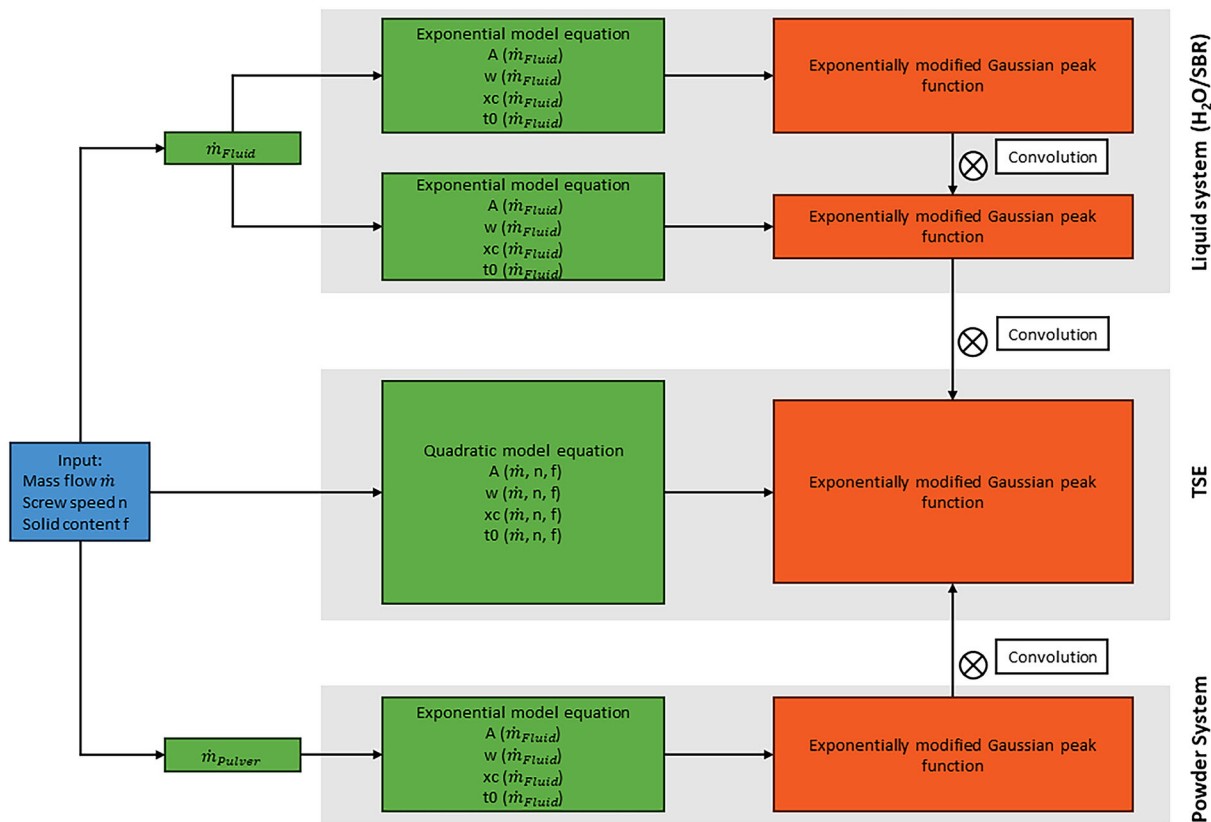


Figure 8. Structure of the entire RTD model based on the submodels for determining $E(t)$ of the continuous mixing process.

Table 5. Experimental points for validating the process section RTD model.

Points	Screw speed n [1/min]	Solid content f [%]	Mass flow \dot{m} [kg h ⁻¹]
Val1	750.00	43	11.00
Val2	567.57	25	7.35
Val3	932.43	45	14.65
Val4	1200.00	35	9.00

four validation points (Table 5). In the slurry recipe of the research project for agile production of battery cells (AgiloBat2, funding code: 03XP0369A), the solid content is 43%. Therefore, this solid content is chosen for one of the four validation points (Val1). The other validation points are chosen so that all the process parameters are varied. It is ensured that they are within the cube of the BBD experimental design and in different corners.

These validation points were simulated and then compared to the real curves. The results are shown in Figure 9. The green curve represents the fluctuating experimental conductivity data, while the blue curve represents the simulated values.

For the validation point Val1, the green and blue curves are close together, especially as the normalized conductivity increases. The time of the peak of the experimentally determined curves is $t_{peak,real} = 57.54$ s and thus 3.88 s behind the peak of the simulation. This corresponds to a relative deviation of 6.74%. The mean residence time of the experimentally determined curves is $t_{m,real} = 64.99$ s. The residence time of the simulation is $t_{m,sim} = 61.60$ s. This is an absolute deviation of 3.39 s and a relative deviation of 5.22%. Both curves are almost identical, which indicates a high model quality. The other validation points also show a high simulation accuracy, as shown by the quantitative analysis of the blue and green lines. The comparison results of the three additional validation points are summarized in Table 6. The analysis shows that the deviations between the experiment and simulation are small for all validation points.

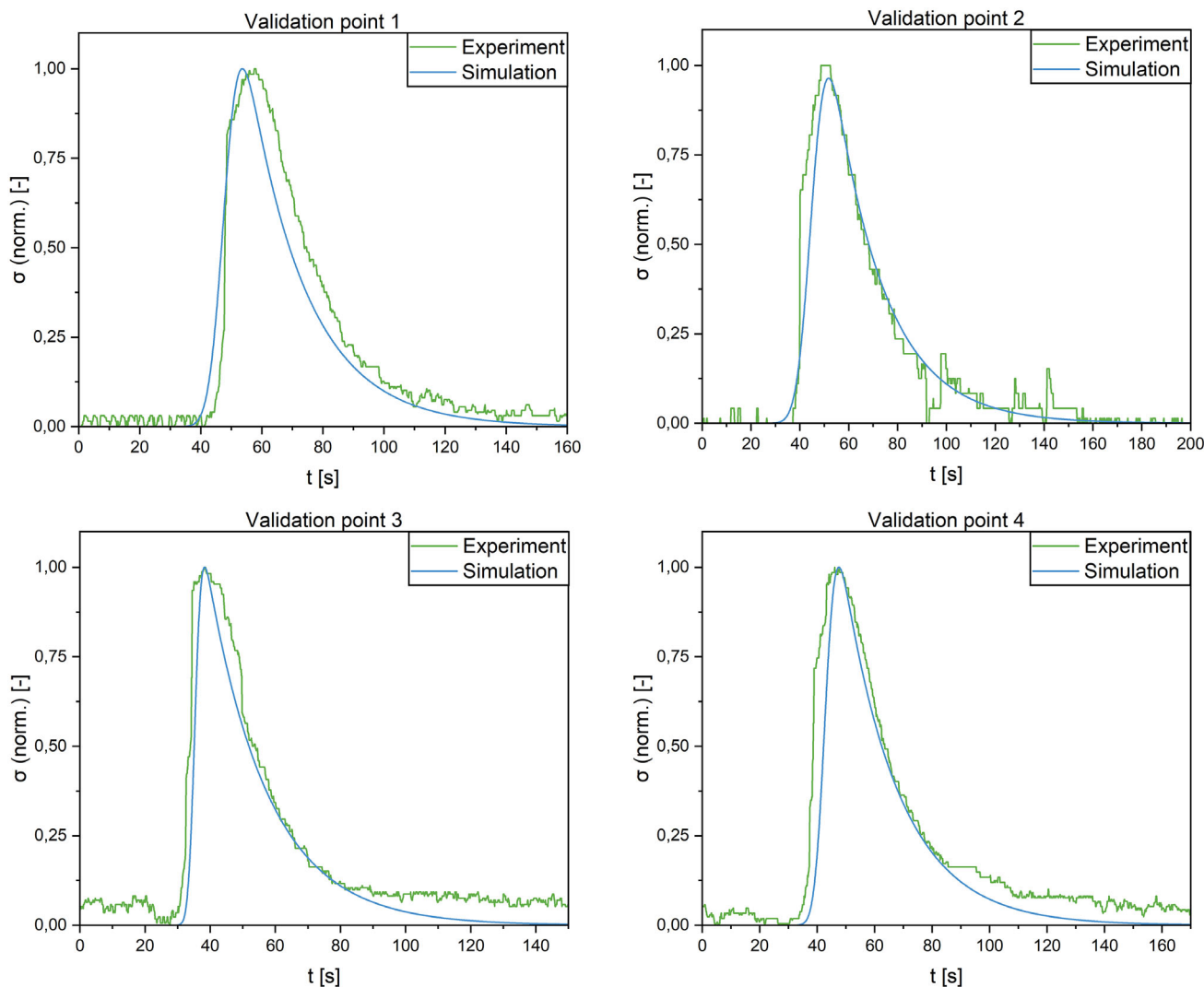


Figure 9. Comparison plots for experimental (green) and simulated (blue) curves for the four validation points.

Table 6. Comparison of real and simulated mean residence time t_m for the process section.

Points	$t_{m,real}$ [s]	$t_{m,sim}$ [s]	Δt [s]	Relative deviation [%]	MSE [s ²]
Val1	64.99	61.60	3.39	5.21	0.00656
Val2	58.50	60.04	1.54	2.63	0.00420
Val3	48.29	48.19	0.10	0.21	0.00675
Val4	57.11	56.47	0.64	1.13	0.00856

The relative deviation of the mean residence times remains below 6%, indicating a high degree of fit between the model and experiment. The smallest deviation was found for validation point Val3, with a relative difference of 0.21%, corresponding to an absolute deviation of 0.1 s.

In addition, the mean square error (MSE) between the experiment and simulation is calculated (Table 6). An ideal simulation would have an MSE of zero. For the validation point Val1, the MSE is 0.00656 s², while for Val2 a lower value of 0.00412 s² was determined, indicating a higher model accuracy in this case. The validation points Val3 and Val4 have MSE values of 0.00675 s² and 0.00856 s². These results confirm that the RTD model accurately simulates the experimental data.

7.2. RTD Model Validation of the Liquid Systems and Hose

As mentioned before, the curve parameters A , x_c , and t_0 show a high prediction precision with a mean deviation of less than 5%. Only parameter w shows a larger deviation of 18%. The effect of this deviation on the RTD is shown in **Figure 10**, where the experimentally determined RTD curve (green) is compared with the simulated RTD curve (blue). For better comparability, the measured conductivity was normalized to the range of 0–1 and then divided by the area under the curve. The minimum residence time of the experimental curve is $t_{m,real} = 130$ s, while it is lower in the simulated curve at $t_{m,sim} = 90$ s. This deviation is

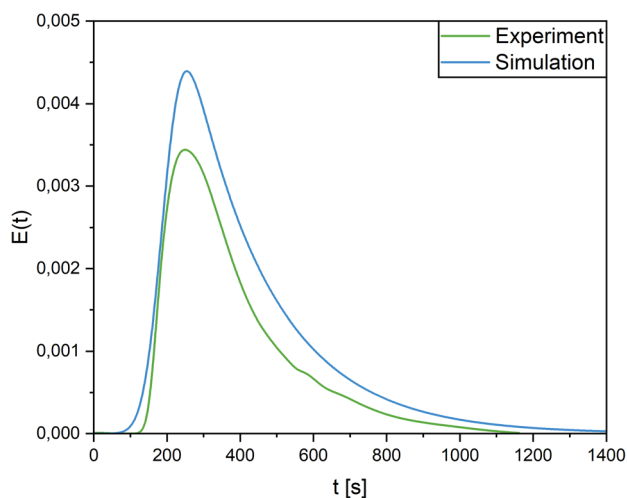


Figure 10. Comparison of the simulation with the actual RTD in the solvent dosing unit at a water mass flow rate of 6.34 kg h⁻¹.

acceptable, as from a process perspective it is more important to remove material too early than to feed potentially bad material to the subsequent process. The maximum peak of the RTD occurs almost simultaneously for the experimental curve at $t_{peak,real} = 249$ s and for the simulated curve at $t_{peak,sim} = 253$ s. However, this deviation has only a small influence on the mean residence time: at a mass flow of 6.34 kg h⁻¹, the experimentally determined mean residence time is $t_{m,real} = 346$ s, while the simulated $t_{m,sim} = 349$ s is only 3 s higher. This corresponds to a relative deviation of only 0.87%, which confirms the high accuracy of the prediction model for the solvent dosing unit.

7.3. RTD Model Validation of the Powder Dosing Unit

In the powder feeder, the RTD typically shows a bimodal curve. This behavior is due to the presence of a core flow within the hopper and feeder unit, as described in Section 5.

The modeling of the first peak has proven to be accurate, as shown in **Figure 11**. Both the shape of the curve and the position of the peak correlate well with the experimental data. The second peak, however, shows more variability due to the complex interaction of factors such as powder flow behavior, residual moisture, powder bridging, fill level, and agitator configuration. While accurate simulation of this second peak remains a challenge, the current approach effectively approximates the shape of the first peak as the most important part.

To further improve the accuracy of the model, a more detailed analysis of the powder flow behavior is required. Particle-based modeling of flow paths, which could provide deeper insight into the formation of the second peak, is a promising area of future research.

7.4. Entire Model Validation

After the individual submodels have been validated and show a very high accuracy, the validation of the entire RTD model is performed. The quality of the model is shown here following the

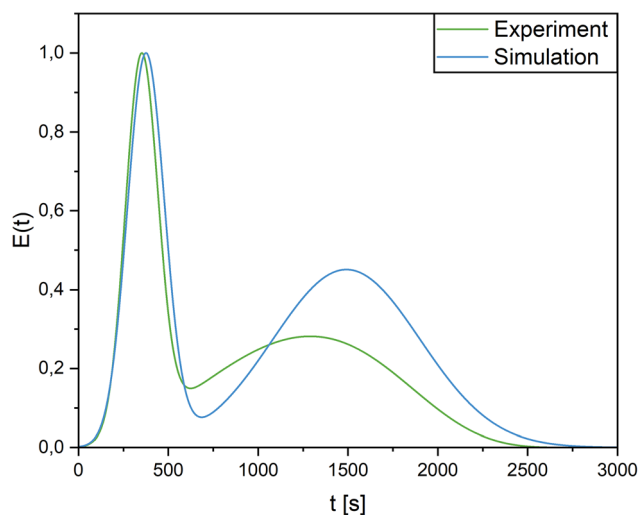


Figure 11. Comparison of the simulation with the actual RTD in the powder dosing unit at a powder mass flow rate of 11.77 kg h⁻¹.

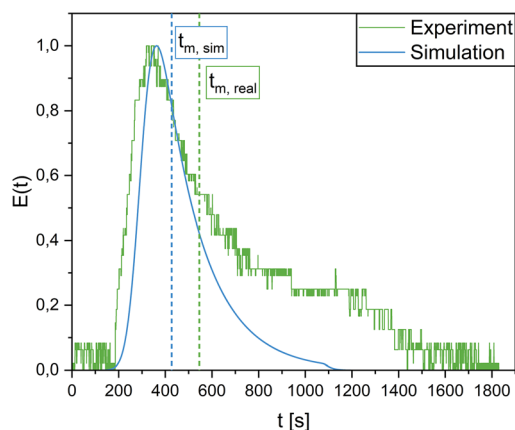


Figure 12. Comparison of the experimental curve (orange) with the simulated and predicted curve (blue) of the RTD.

material flow path of the solvent. The process parameters selected are parameters that are not used to develop the submodels and only used for model validation. In addition, the selected process parameters represent a realistic process operating point, which is also used in a similar way in an industrial production.

To record the experimental residence time curve, 20 mL tracer was added impulsively with a pipette at position C (Figure 1). The tracer concentration is measured at the outlet of the TSE at position Z (Figure 1). **Figure 12** shows the comparison of the measured normalized conductivity (orange) and the simulated normalized conductivity (blue). The fluctuation in the orange curve is due to the resolution of the conductivity sensor. The tracer is added at $t = 0$ s.

For the experimental curve, the minimum residence time is $t_{\min, \text{real}} = 188.09$ s. The peak is reached at $t_{\text{peak}, \text{real}} = 333.28$ s and the mean residence time is $t_{m, \text{real}} = 545.8$ s. A comparison with the simulated residence time curve (blue) shows that the curves are similar, especially up to $t = 500$ s. After that, there is a deviation between the curves, so that $t_{\max, \text{sim}} = 1209.9$ s and $t_{\max, \text{real}} = 1829.04$ s. This difference can be explained by the fact that due to dead zones, turbulence and back mixing, the material can remain at certain points longer than estimated by the simulation. This is especially expected at transition points from one subsystem to the next and at sharp edges. However, when looking at the characterizing and important times t_{\min} and t_{peak} , it becomes clear that the deviation is only marginal. The deviation of $t_{m, \text{sim}}$ can be explained as follows: the individual submodels already show minimal deviations, which are increased by the mathematical convolution operation. This is where the shift occurs. However, it should be noted that from a process engineering point of view it is more important that the simulated t_{\min} , t_{peak} , and t_m are ahead of the real-time values, as this is the only way to ensure that, i.e., scrap is ejected in time. For this reason, the deviation is not considered to be critical.

Optimization of the existing model, especially with regard to the curve progression and the associated difference in t_{\max} , seems to be beneficial. Here, it is important to investigate whether using a parameter-dependent stretching factor already offers a higher prediction accuracy for the curve progression after the time t_m and whether the difference for t_m can be reduced as a result.

8. Conclusion

A model developed from experimental data is presented that predicts the RTD of a TSE based on the input process parameters of screw speed, mass flow, and solid content. This is possible for the entire mixing system and the process section, solvent dosing unit, binder dosing unit, and powder dosing unit. The simulation models show a high degree of accuracy for RTD simulation of the solvent water and binder solution in the liquid dosing unit and the process section. The use of an exponential model equation is found to be suitable for accurately simulating the RTD in the solvent dosing unit and binder dosing unit.

As a result, the residence times can be simulated with a very high degree of accuracy from when the raw materials are added to the end of the continuous mixing process. This precise simulation enables process optimization and minimizes material waste by allowing the selective separation of nonconforming material, thereby reducing scrap to a minimum. In addition, the RTD model makes it possible for the first time to provide traceability in the continuous slurry mixing process in battery cell production.

Based on the results presented, future research should investigate the effects of different screw configurations, process parameters like temperature, shear rate, etc. and product parameters like viscosity on the RTD, as variations in design and process are expected to affect material flow and mixing behavior significantly. In addition, the effects of recipe changes particularly change in mass content and component ratios for slurries or alternative materials should be investigated to evaluate the robustness of the model. Further studies should also focus on the transferability of the RTD model to cathode production and novel dry mixing techniques that are fundamentally different from conventional slurry-based processes.

Appendix

Table 7. Experimental points of the Box–Behnken design.

Point	n [rpm]	\dot{m} [kg h ⁻¹]	f [%]
BBD1	482.43	11.00	20
BBD2	482.43	11.00	50
BBD3	482.43	5.65	35
BBD4	482.43	16.35	35
BBD5	750.00	5.65	20
BBD6	750.00	5.65	50
BBD7	750.00	16.35	20
BBD8	750.00	16.35	50
BBD9	750.00	11.00	35
BBD10	750.00	11.00	35
BBD11	750.00	11.00	35
BBD12	1017.57	11.00	20
BBD13	1017.57	11.00	50
BBD14	1017.57	5.65	35
BBD15	1017.57	16.35	35

Acknowledgements

The authors would like to express their appreciation to the German Federal Ministry of Education and Research (BMBF) for supporting the project “IntelliPast” (funding code: 03XP0343A) and the project “AgiBat2” (funding code: 03XP0369A). This work contributes to the research performed at KIT-BATEC (KIT Battery Technology Center) and at CELEST (Center for Electrochemical Energy Storage Ulm Karlsruhe). The authors would like to thank Julia Maelger and Marc Hoffmann for their contributions to the subject matter.

Open Access funding enabled and organized by Projekt DEAL.

Conflict of Interest

The authors declare no conflict of interest.

Author Contributions

Simon Otte: formal analysis (lead); investigation (lead); methodology (lead); software (lead); validation (lead); visualization (lead); writing—original draft (lead); writing—review and editing (lead). **Sebastian Schabel:** writing—review and editing (supporting). **Jürgen Fleischer:** funding acquisition (lead); supervision (lead); writing—review and editing (supporting).

Data Availability Statement

The data that support the findings of this study are available from the corresponding author upon reasonable request.

Keywords

battery cell production, continuous processes, extrusion, mixing, modeling, residence time distribution, slurries, traceability

Received: February 28, 2025

Revised: June 3, 2025

Published online:

- [1] *Roadmap Batterie-Produktionsmittel 2030. Update 2023*, Frankfurt am Main, **2023**.
- [2] C. Dahmen, F. Degen, M. C. Eckstein, K. B. Pouls, H. Walter, R. Ludwigs, A. Scheibe, *Mastering Ramp-up of Battery Production*, Fraunhofer-Gesellschaft **2024**.
- [3] H. Dreger, H. Bockholt, W. Haselrieder, A. Kwade, *J. Electron. Mater.* **2015**, *44*, 4434.
- [4] J. Li, J. Fleetwood, W. B. Hawley, W. Kays, *Chem. Rev.* **2022**, *122*, 903.
- [5] S. Otte, N. N. A. M. Sufian, S. Schabel, J. Fleischer, *Energy Technol.* **2024**, 2400493.
- [6] M. Haarmann, W. Haselrieder, A. Kwade, undefined **2019**.
- [7] J.-H. Schünemann, H. Dreger, H. Bockholt, A. Kwade, *ECS Trans.* **2016**, *73*, 153.
- [8] A. Kwade, W. Haselrieder, R. Leithoff, A. Modlinger, F. Dietrich, K. Droeder, *Nat. Energy* **2018**, *3*, 290.
- [9] P. Wunderlich, N. Ehteshami-Flammer, J. Krauß, A. Fitzner, L. Mohring, C. Dahmen, *The Power of Digitalization in Battery Cell Manufacturing* **2024**.
- [10] M. M. Nasr, M. Krumme, Y. Matsuda, B. L. Trout, C. Badman, S. Mascia, C. L. Cooney, K. D. Jensen, A. Florence, C. Johnston, K. Konstantinov, S. L. Lee, *J. Pharm. Sci.* **2017**, *106*, 3199.
- [11] M. Haarmann, D. Grießl, A. Kwade, undefined **2021**.
- [12] J. F. Meza Gonzalez, H. Nirschl, *Energy Technol.* **2023**, *11*, 1.
- [13] A. Buss, J. P. Doppler, I. Effenberger, D. Ensling, C. Haar, S. Hartleif, G. Rixinger, K. Schöbel, M. Trierweiler, T. Bauernhansl, *Handbook on smart battery cell manufacturing. The power of digitalization* (Eds.: P. Birke, M. Weeber, M. Oberle), WORLD SCIENTIFIC, New Jersey, London, Singapore, Beijing, Shanghai, Hong Kong, Taipei, Chennai, Tokyo, **2022**, pp. 123.
- [14] G. Rixinger, J. P. Doppler, C. Haar, M. Trierweiler, A. Buss, K. Schöbel, D. Ensling, T. Bauernhansl, *Integration of Traceability Systems in Battery Production* **2020**.
- [15] A. Sommer, S. Bazlen, H.-Y. Tran, W. Braunwarth, R. Daub, *Proc. CIRP* **2023**, *120*, 171.
- [16] S. Otte, J. Maelger, S. Schabel, H. Nirschl, J. Fleischer, *Energy Technol.* **2025**, 202402196.
- [17] P. V. Danckwerts, *Chem. Eng. Sci.* **1953**, *50.24*, 3857.
- [18] J. Peng, H. E. Huff, F. Hsieh, *J. Food Process. Preserv.* **1994**, *18*, 263.
- [19] M. Baerns, A. Behr, A. Brehm, J. Gmehling, K.-O. Hinrichsen, H. Hofmann, R. Palkovits, U. Onken, A. Renken, *Technische Chemie*, Wiley-VCH, Weinheim, **2013**.
- [20] O. Levenspiel, *Chemical Reaction Engineering*, Wiley, Hoboken, NJ, **1999**.
- [21] Y. Gao, F. J. Muzzio, M. G. Ierapetritou, *Powder Technol.* **2012**, *228*, 416.
- [22] B. Platzer, *Chem. Ing. Tech.* **1996**, *68*, 769.
- [23] C. G. Gutierrez, E. F. Dias, J. A. Gut, *J. Food Eng.* **2010**, *98*, 248.
- [24] J. Nassauer, *Dissertation*, Technische Universität München, München, **1978**.
- [25] E. Salamí, *Dissertation*, Eidgenössische Technische Hochschule Zürich (ETH Zürich), Zürich, **1968**.
- [26] J.-H. Ham, B. Platzer, *Chem. Eng. Technol.* **2004**, *27*, 1172.
- [27] J. R. Hart, I. Guymer, F. Sonnenwald, V. R. Stovin, *J. Hydraul. Eng.* **2016**, *142*.
- [28] M. Peterwitz, J. Jodwirschat, R. Loll, G. Schembecker, *Int. J. Pharm.* **2022**, *614*, 121467.
- [29] P. Bhalode, S. M. Razavi, A. Roman-Ospino, J. Scicolone, G. Callegari, G. Tian, A. Koolivand, S. Krull, M. G. Ierapetritou, F. J. Muzzio, *Int. J. Pharm.* **2023**, *634*, 122653.
- [30] J. Gao, G. C. Walsh, D. Bigio, R. M. Briber, M. D. Wetzel, *AIChE J.* **1999**, *45*, 2541.
- [31] S. M. Razavi, A. D. Román-Ospino, P. Bhalode, J. Scicolone, G. Callegari, A. Dubey, A. Koolivand, S. Krull, G. Tian, X. Xu, T. O' Connor, M. Ierapetritou, F. Muzzio, *Powder Technol.* **2023**, *429*, 118864.
- [32] M. S. Escotet-Espinoza, S. Moghtadernejad, S. Oka, Y. Wang, A. Roman-Ospino, E. Schäfer, P. Cappuyns, I. van Assche, M. Futran, M. Ierapetritou, F. Muzzio, *Powder Technol.* **2019**, *342*, 744.
- [33] M. S. Escotet-Espinoza, S. Moghtadernejad, S. Oka, Z. Wang, Y. Wang, A. Roman-Ospino, E. Schäfer, P. Cappuyns, I. van Assche, M. Futran, F. Muzzio, M. Ierapetritou, *Powder Technol.* **2019**, *344*, 525.
- [34] B. van Snick, A. Kumar, M. Verstraeten, K. Pandelaere, J. Dhondt, G. Di Pretoro, T. de Beer, C. Vervae, V. Vanhoorne, *Int. J. Pharm.* **2019**, *556*, 200.
- [35] W. Engisch, F. Muzzio, *J. Pharm. Innov.* **2016**, *11*, 64.
- [36] “Methoden und Formeln für Statistiken für die Güte der Anpassung in Wirkungsflächenversuchsplan analysieren - Minitab”, can be found under <https://support.minitab.com/de-de/minitab/help-and-how-to/statistical-modeling/doi/how-to/response-surface/analyze-response-surface-design/methods-and-formulas/goodness-of-fit-statistics/>, 2024.
- [37] M. Werner, *Digitale Bildverarbeitung. Grundkurs mit neuronalen Netzen und MATLAB®-Praktikum*, Springer Vieweg, Wiesbaden **2021**.